

Green's Function Measurements of Force Transmission in 2D Granular Materials

Junfei Geng^a, G. Reydellet^b, E. Clément^b, R. P. Behringer^{a,*}

^a*Center for Nonlinear and Complex Systems, Duke University, Durham NC, 27708-0305, USA*

^b*Université Pierre et Marie Curie, Paris 75231, France*

Abstract

We describe experiments that probe the response to a point force of 2D granular systems under a variety of conditions. Using photoelastic particles to determine forces at the grain scale, we obtain ensembles of responses for the following particle types, packing geometries and conditions: monodisperse ordered hexagonal packings of disks, bidisperse packings of disks with different amount of disorder, disks packed in a regular rectangular lattice with different frictional properties, packings of pentagonal particles, systems with forces applied at an arbitrary angle at the surface, and systems prepared with shear deformation, hence with texture or anisotropy. We experimentally show that disorder, packing structure, friction and texture significantly affect the average force response in granular systems. For packings with weak disorder, the mean forces propagate primarily along lattice directions. The width of the response along these preferred directions grows with depth, increasingly so as the disorder of the system grows. Also, as the disorder increases, the two propagation directions of the mean force merge into a single direction. The response function for the mean force in the most strongly disordered system is quantitatively consistent with an elastic description for forces applied nearly normally to a surface, but this description is not as good for non-normal applied forces. These observations are consistent with recent predictions of Bouchaud et al. [Bouchaud et al., *Euro. Phys. J.* **E4** 451 (2001); Socolar et al., *Euro. Phys. J.* **E7** 353 (2002)] and with the anisotropic elasticity models of Goldenberg and Goldhirsch [Goldenberg & Goldhirsch, *Phys. Rev. Lett.* **89** 084302 (2002)]. At this time, it is not possible to distinguish between these two models. The data do not support a diffusive picture, as in the q -model, and they are in conflict with data by Rajchenbach [Da Silva & Rajchenbach, *Nature* **406** 708 (2000)] that indicate a parabolic response for a system consisting of cuboidal blocks. We also explore the spatial properties of force chains in an anisotropic textured system created by a nearly uniform shear. This system is characterized by stress chains that are strongly oriented along an angle of 45° , corresponding to the compressive direction of the shear deformation. In this case, the spatial correlation function for force has a range of only one particle size in the direction transverse to the chains, and varies as a power law in the direction

of the chains, with an exponent of -0.81. The response to forces is strongest along the direction of the force chains, as expected. Forces applied in other directions are effectively refocused towards the strong force chain direction.

Key words: Granular materials; Stress chains; Response functions; Photoelasticity
PACS: 46.10.+z; 47.20.-k

1 Introduction

Force propagation in granular materials is a fundamental, but unresolved problem[1,2] which has received much recent attention[3,4,5,6,7,8,9,10,11,12]. Several features of granular materials are responsible for the complexity of the problem. One of these is the fact that typical materials do not exist in ordered states. Here, order or disorder involves several aspects. The packing of grains is usually not in an ordered lattice. In addition, even packings with a high degree of spatial packing order need not have order in the forces at the particle contacts. One cause of disorder is redundancy of contacts, i.e. the fact that packings may have more contacts than are needed for mechanical stability. For example, in a hexagonal packing of ideal disks, each disk except those at boundaries may have as many as six contact points, while the conditions of force and torque balance (in 2D) require four contacts, i.e. two contacts located below the center of gravity of each disk (hyperstatic equilibrium[13]). In real packings, it is often possible that each particle (even a particle with low friction) can randomly lose several contacts without destroying the stability of the lattice. Conversely, even in a packing of frictionless particles, there can be a substantial range of forces at contacts, with a high degree of randomness. If friction is introduced, non-normal forces are allowed, the number of degrees of freedom increases, and effectively, the conditions for stability are relaxed even further. The frictional forces at grain contacts provide an additional source of complexity: static frictional contacts are history-dependent. Hence, a seemingly “ordered” system from the point of view of geometrical packing can contain disorder in the contact forces, due to small shape and size variation of disks and, more importantly, to the existence of friction[4,14,15,16,17]. In addition, forces at contacts are nonlinear, first, because forces vanish once a contact is broken, and second, because in many cases, particles that are in contact repel each other with normal forces that vary nonlinearly with the inter-particle center of mass separation. At the mesoscopic level, even a nominally uniform applied external stress results in a filamentary network of

* Corresponding author.

Email address: bob@phy.duke.edu (R. P. Behringer).

stress/force chains[18], where a modest fraction of the total number of grains carry the majority of the force. We show an example of these chains in Fig. 21.

Repetition of experiments under identical macroscopic conditions typically leads to substantially different stress chain patterns each time. This large variability under repetition suggests that a statistical approach might be the most appropriate one. This approach might take the form of averaging a single realization over large regions of space. Alternatively, it might take the form of an ensemble of measurements under identical macroscopic conditions. The assumed validity of the former is implicit in typical macroscopic models of stress propagation for granular materials. Here, we take the second approach. By determining an ensemble of responses at the microscale, we not only determine average behavior, we also determine the range of possible behavior and the probability of obtaining a particular response to an applied stress or force.

A number of substantially different models[6,7,8,10,19,20,21,22,23] exist to characterize force propagation in dense granular materials, ranging from lattice[7,20,22] to continuum[19] descriptions. The range of predictions is underscored by noting that in the continuum case, various models involve PDE's of totally different type. For example, classical elastoplastic models[19], are described by elliptic equations below the plastic threshold (which is the region we consider here) or hyperbolic equations above the plastic threshold. The continuum limit of the q-model of Coppersmith et al.[20]. is a parabolic PDE. The oriented stress linearity (OSL) model[21] of Bouchaud et al. is based on a hyperbolic PDE. These authors have further explored force propagation through lattice models which predict a wave equation for stress propagation for ordered systems, a convection-diffusion equation for weak disorder, and eventually, a transition to elliptic PDE's in the presence of stronger disorder.

Very recently, two substantially different models have been proposed to account for recent measurements[3,4]. One is the force chain splitting model or double-Y model of Bouchaud et al.[6,7] which is a Boltzmann equation for the probability density of force chains with a given intensity and orientation. In the presence of strong disorder and isotropic “scattering” of force chains, the authors derive stress equations formally identical to those of classical elasticity. An alternative model by Goldenberg and Goldhirsch[8] assumes that nearest neighbors in a 2D packing of disks are coupled by bi-directional or uni-directional linear springs. These authors propose that the experimental results can be described using anisotropic elasticity, leading to a PDE of elliptic type in the continuum limit. Very recently, there has been further exploration of elasticity models by Otto et al. [24].

Another important aspect of the problem concerns textures in a granular system. Texture refers to the distribution of contacts between grains, and it is defined at the local scale, in terms of the dyadic tensor formed from the

components of the unit vectors between the contacts experienced by particle and its center of mass [2,25,26]. Specifically, a fabric tensor representing the distribution of contacts can be defined by the dyadic product[25,26]:

$$F_{xy} = \langle n_x^\alpha n_y^\alpha \rangle . \quad (1)$$

Here, $\vec{n}^\alpha = n_x^\alpha \hat{x} + n_y^\alpha \hat{y}$ is the unit vector from the center of mass of the particle to the α 'th contact point, and the angle brackets represent an average over all contact points on the particle. Both experiments and numerical simulations[27,28,12,29,30] have shown that the existence of non-isotropic textures due to different deposition procedures of sandpiles or other packing procedures can determine the way forces are transmitted and produce different stress distributions. Among recent models, the force chain splitting model emphasizes the need to incorporate a texture[6]. The spring model by Goldenberg and Goldhirsch[8] explores the possibility of anisotropic elasticity associated with texture to account for the features observed in experiments on ordered systems, where forces tend to propagate along principal lattice directions.

A useful experimental tool for distinguishing among these models is the response function for a localized force[2]. To the extent that this response is linear, it corresponds to an experimental realization of the force Green's function. In previous work[3,4], we investigated one of the simplest cases: response to a small force applied normally at the boundary of 3D and 2D systems. We showed that spatial ordering of the particles is a key factor: 2D ordered packings respond strongly along the lattice directions, whereas disordered packings show a broad elastic-like response both in 2D and 3D. Other recent experiments by Rajchenbach[5] involved a packing of rectangular blocks, and the measured response was consistent with a diffusive description. The reasons for the disagreement between our experiments and those of Rajchenbach remain unexplained, but may be related to the differences in the particle types used in the two different experiments. Recently, Mueggenburg et al.[12] reported measurements on ordered and disordered 3D packings. They found for disordered packings that there was a broad central response to a point force, but the dependence of the width on depth was not sufficiently well resolved to distinguish between elastic vs. diffusive descriptions. For ordered packings, they found propagation along preferred directions. However, the nature of these directions and the amount of spreading of the response depended crucially on the packing structure. FCC packings showed force transmission along three well defined lines with moderate broadening with depth. By contrast, HCP packings showed substantially more broadening with depth, and the preferred transmission was along cones. These authors have interpreted their results in terms of the packing geometry: for their FCC packings, they note the presence of direct lines along which the forces could propagate, whereas in their HCP packings, such paths did not exist.

This paper further explores through experiments the issues of the local response of granular materials to small forces. We consider the regime of limited deformation, so that to a reasonable approximation, our results represent a true Green's function. We present information on the methods used and we explore a broad range of systems. In particular, we consider: 1) responses of monodisperse disks in ordered hexagonal packings, 2) bidisperse systems with different amount of disorder, 3) responses of systems of pentagonal particles—systems that are primarily disordered, 4) responses of rectangular packings of disks where we vary the inter-particle friction, 5) responses to forces applied at arbitrary angles to the surface, and 6) responses of a previously sheared, thus textured/anisotropic, system.

The organization of this work is as follows. In Section 2, we describe experimental procedures, methods and issues common to all experiments. In Section 3, we describe a variety of experiments. Finally, we draw conclusions in Section 4.

2 Techniques, procedures and common features

In this section, we describe procedures and analysis methods common to all the experiments described here. We also address the issue of linearity in the force response. An additional issue that is common to all these experiments, which we discuss briefly in this section, is the nature and importance of fluctuations.

2.1 *Experimental procedures*

2.1.1 *Experimental arrangements*

Photoelastic measurements[31], involving stress-induced birefringence provide in 2D a unique opportunity to obtain information about the internal structure of granular materials. The experiments we describe below typically use a layer of photoelastic grains consisting of either disks or pentagonal particles. All the particles are cut from flat sheets of a commercially available material (Measurements Group, Inc. material PSM-4) with a Young's modulus of 4 MPa and a Poisson ratio between 0.4 and 0.5.

The grains are arranged in one of two configurations. In one, they are contained between two transparent Plexiglas sheets; in the second, the particles lean very gently against a glass plate that is inclined by about 2° from vertical, so that the grains are supported, but with minimal friction with the support-

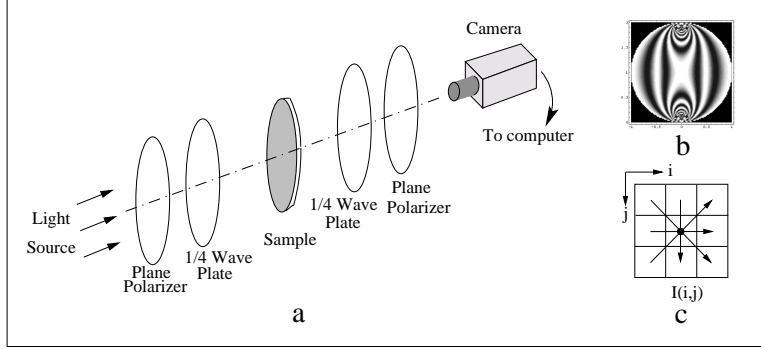


Fig. 1. a) Schematic view of the circular polarimeter setup. In our experiment each linear polarizer and quarter wave plate is combined into a single sheet. b) Expected fringe pattern of a disk under diametrical compression. c). Schematic drawing of how we calculate G^2 .

ing plate. In either case, the assembly is placed between a pair of left- and right-hand circular polarizers as shown in Fig. 1a. Light passes through this sandwich to produce a polariscope intensity image. We record these images with a digital camera at a resolution of 640×480 pixels. For illumination, we use a light box such as that used to read x-ray films, because this provides a relatively homogeneous source. When the photoelastic grains are subjected to stresses, they become birefringent; the resulting transmitted intensity is a measure of the applied stress, as specified in more detail below. Fig. 1b shows a typical intensity picture for a disk under diametrical compression observed with polarizers.

When we use a vertical arrangement, the effect of hydrostatic head must be removed. We note that most experiments were performed with such an orientation because then the effects of friction with the supporting plate are too small to be relevant.

2.1.2 Force measurement

A key issue is how to deduce forces on a particle, i.e. forces at a grain scale. When light travels through the particles along the direction normal to the plane of the experiment, the emerging light intensity, I , in a circular polariscope image is a function of the stress in the plane of the disks at each position (x, y) , as in Fig. 1b. Specifically, the local light intensity is given by

$$I(x, y) = I_o \sin^2[(\sigma_2 - \sigma_1)tC/\lambda], \quad (2)$$

where the I_o is the incident light intensity, σ_1 and σ_2 are the principle stresses at position (x, y) , t is the thickness of the sample, C is the stress optic coefficient, and λ is the wavelength of the light. In typical photoelastic images of the particles, bands corresponding to different values of $(\sigma_2 - \sigma_1)$ occur,

where neighboring bright bands are separated by a phase difference of π in the argument of the sine function above.

In general, the complete inverse problem that extracts vector forces on a particle for a given photoelastic image is a formidable problem. In these experiments, we use an empirical approach that allows us to obtain force at the grain scale with reasonable accuracy and is much simpler than a complete calculation. The basis for this process is the fact that as the applied force at contact increases, the number of fringes (black or white bands) also increases monotonically. We exploit this fact to produce a force calibration in terms of a quantity that we denote by G^2 :

$$G^2 \equiv |\nabla I|^2 = \left[\left(\frac{I_{i-1,j} - I_{i+1,j}}{2} \right)^2 + \left(\frac{I_{i,j-1} - I_{i,j+1}}{2} \right)^2 + \left(\frac{I_{i-1,j+1} - I_{i+1,j-1}}{2\sqrt{2}} \right)^2 + \left(\frac{I_{i-1,j-1} - I_{i+1,j+1}}{2\sqrt{2}} \right)^2 \right] / 4, \quad (3)$$

where $I_{i,j}$ is the intensity at pixel (i, j) , as shown in Fig. 1c. The indices i, j are the discrete replacement of the continuous variables x, y . Note that to avoid directional preference, the vertical, horizontal, and both diagonal gradients are squared and averaged with appropriate weights. We first compute $G^2(i, j)$ for each pixel (i, j) . Then, for a particle or collection of particles covered by N pixels we calculate the average square gradients:

$$\langle G^2 \rangle = \frac{1}{N} \sum_{k=1}^N |\nabla I_k|^2. \quad (4)$$

As the number of fringes increase, so does this average square gradient. The method can be applied to calibrate the mean force on a single particle or a larger assembly of particles. We obtained calibrations by either: (1) applying known forces to the boundary of a small number of particles and at the same time measuring $\langle G^2 \rangle$, or (2) by applying various uniform loads to the upper surface of a large rectangular sample (width larger than height to avoid the Janssen effect) as shown in Fig. 2b. We show here a calibration curve, Fig. 2(a) inset, using the second method.

The validity of the G^2 calibration method is also tested by measuring the hydrostatic pressure vs. depth z . In a static system without external load, the hydrostatic pressure due to gravity is: $P = \gamma \rho g t z$, where ρ is the density of the material from which the particles are made, g is gravity and γ is the packing fraction of the particles. In the experiment, the density, ρ , is $1.15 \times 10^3 \text{ Kg} \cdot \text{m}^{-3}$ and the typical packing fraction γ is ~ 0.75 for pentagons and 0.91 for hexagonally packed disks. The expected curves, based on the calibration of

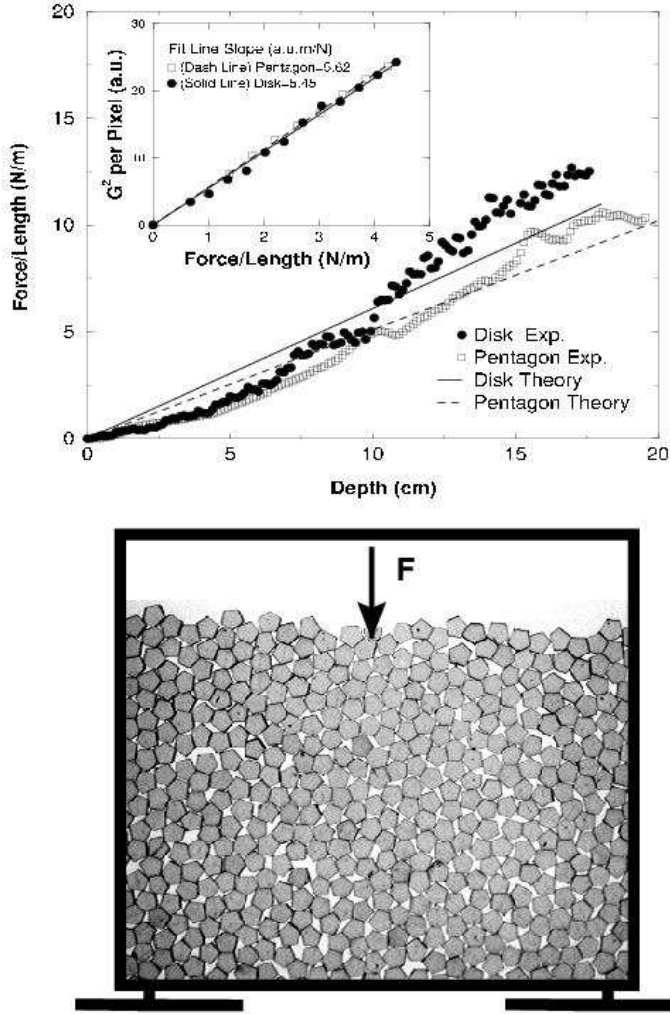


Fig. 2. a) Hydrostatic pressure due to gravitational force alone versus depth determined from G^2 . The expected slopes of the stress-height curves are calculated from the known packing fraction ($\gamma = 0.91$ for disks; $\gamma \simeq 0.75$ for pentagons). Inset shows the multi-particle G^2 calibration by applying known loads to the upper surface of the layer. b) Schematic of the experimental apparatus with an overlay showing an image of an actual packing of pentagonal particles. The drawing is not to scale. The width is about three times the height in the actual experiment, in order to avoid boundary effects. F is the applied vertical load.

Fig. 2a-inset, and experimental hydrostatic head data obtained from the G^2 method, shown in Fig. 2a, agree well. Thus, a simple interpretation of the G^2 method is that it represents the local pressure (i.e. the trace of the stress tensor). These calibrations are effective until the forces are so large that it is no longer possible to resolve the fringes on a particle clearly, a condition that does not occur in these studies. They are also limited at low forces, since the gradients in that case become weak.

2.1.3 Procedures

A typical procedure was as follows. The particles were first placed in the apparatus. We then obtained a sequence of images. The first image, made in the absence of the applied load, yielded the particle locations. This image was taken without the polarizers in place, and from it, we extracted particle positions and contacts by image analysis. A second image with polarizers in place but no applied load provided the background photoelastic image. We then measured the system point-force response by placing a known weight carefully on top of one particle at the surface or by pushing on one grain with a high precision digital force gauge (model DPS-110 from Imada Inc.). With the local applied force in place, we obtained a second photoelastic image. We then removed the local force and obtained one last image without polarizers to ascertain if there had been any particle movement.

With the exception of packings of bidisperse disks, we did not use trials in which there were changes in the particle packing after the local force was removed. In the case of bidisperse disk packings, some small movement of the particles at the surface typically occurred no matter how weak the applied force. However, this motion was limited to particles very near the surface and the location of the applied force.

By computing G^2 at the pixel scale for each image and subtracting the background from the response with load, we obtained the stress difference between successive images of G^2 , containing only the response from the point perturbation. We refer to this difference as ΔG^2 , or as G^2 in the cases where no confusion is caused.

2.2 A statistical approach

In all cases, the responses differ significantly from realization to realization, a feature that was also considered in recent theoretical work[22]. This is true even for the case of nearly regular grain packings, since the frictional forces at the contacts are determined by the microscopic details of the preparation history, something that in general is not known. Hence, it is necessary to develop an ensemble of measurements under identical macroscopic control conditions in order to extract the mean behavior. In order to obtain such ensembles, we repeated measurements on a given system for many different rearrangements of the particles, typically 50 times for each set of data. Between runs, the system was either “stirred” using a rod or “massaged” using hand to rearrange the particles. For the regularly packed lattices, the goal was to rearrange the forces at the contacts without generally changing the positional order of the particles. For the disordered lattices, the positional order was also

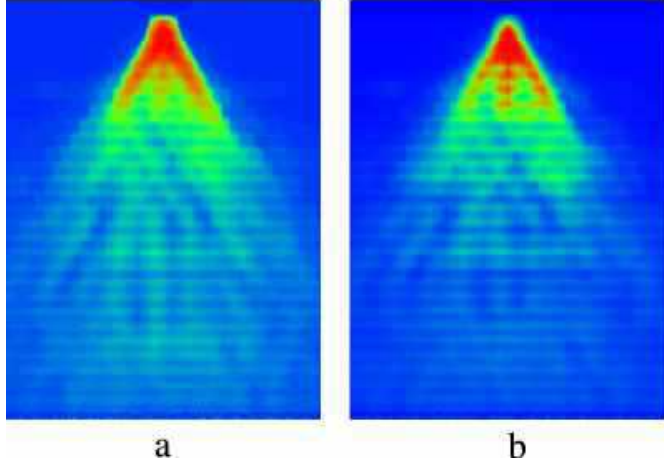


Fig. 3. The mean response, (a), and the standard deviation, (b), of G^2 for a hexagonal packing of disks. The standard deviation image has a similar shape to the mean image.

changed. To make sure that our measurements were statistically significant, we divided 50 measurements into two groups, each consists 25 measurements, and verified that the averaged responses for two groups were consistent.

For responses in each realization, we denote the stress at the pixel scale for a given realization, n , as $G^2(x, y, n)$. To obtain the ensemble mean response, we average in two ways. First, we compute the average of $G^2(x, y, n)$ over n . As noted above, we then carry out a coarse-graining at the scale of a single particle, since variations in G^2 below the particle size are not meaningful here. The result is denoted by $\overline{G^2(x, y)}$.

The ensemble contains important information concerning the range and probability of results that might be encountered at any position (x, y) . To characterize the fluctuations from one realization to another, we calculate the standard deviation of the stress for each position: $rms(x, y) = \sqrt{Var}$, where

$$Var = \frac{1}{N-1} \sum_{n=1}^N (G^2(x, y, n) - \overline{G^2(x, y)})^2. \quad (5)$$

As an example, we show the $rms(x, y)$ for a hexagonal disk packing in Fig. 3b, using a greyscale representation. Here, brighter regions represent larger values of the rms . We contrast the greyscale image for the fluctuations to the mean response in Fig. 3a. The rms image clearly has a similar shape to the mean image, and the similarity in these patterns suggests that there is a simple point-wise relation between these two quantities. We explore this by determining the distribution, without regard to position, of the ratio $rms(x, y)/\overline{G^2(x, y)}$ for all points in the system. The data for the hexagonal packings of monodisperse disks are given by the solid circles in Fig. 4. The distribution has a well

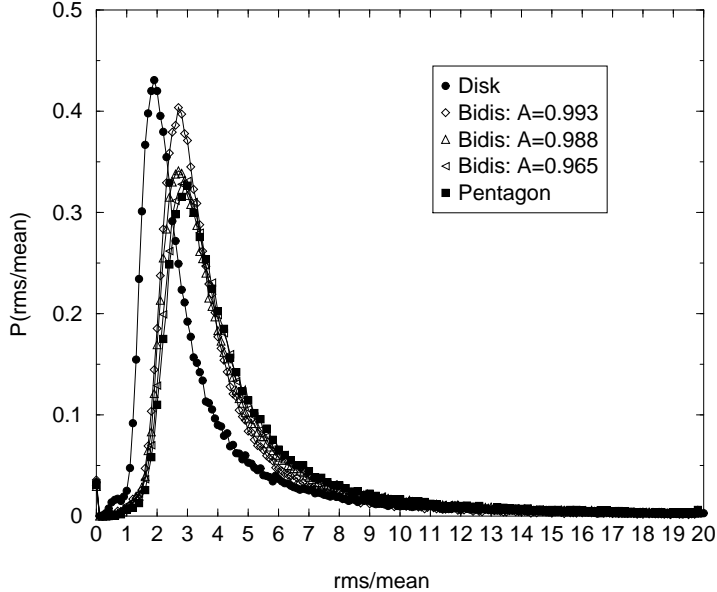


Fig. 4. The distributions of the ratio of standard deviation to the mean G^2 for all points in the system. Each curve represents a different system, as indicated in the inset.

defined peak at around 2, i.e. the most probable occurrence is that the rms is twice the mean. The rest of the curves in Fig. 4 are similar plots for bidisperse systems of disks with different amount of disorder, and for a system of pentagons, systems which we will discuss below. Briefly, the amount of spatial disorder increases as we change the system from monodisperse disks to bidisperse disks and finally to pentagons. As the amount of disorder increases, the peak in the distributions of $rms/\overline{G^2(x,y)}$ shifts to larger values, and the distributions become wider.

2.3 Linearity of the Response

Additional issues that are of considerable importance in all the measurements are reversibility and linearity. The first refers to the fact that the particles return to their unperturbed state after the applied local force is removed. The second concerns the functional relationship between the size of the applied force and the response at a given point. With the exception of bidisperse systems of disks (as noted above) for the measurements reported here, deformations were completely reversible for small forces. For bidisperse packings, the process of adding and removing a point force was reversible except for a few of particles on the surface and near the applied force. The vast majority of the particles, those in the bulk of the sample were undisturbed.

However, reversibility does not necessarily mean linearity. We have carried out systematic tests of the linearity of the response, as shown in Fig. 5. These

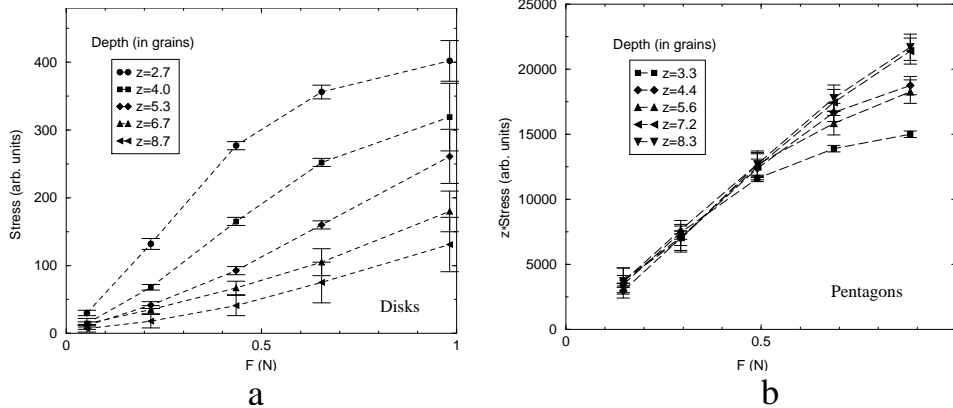


Fig. 5. Linearity test: a) Measured peak stress vs. applied force at different depths along the principal lattice directions in a hexagonally packed monodisperse disk system. b). Measured stress multiplied by the corresponding depth vs. applied force for different depths in a pentagonal system. (See Appendix)

data are discussed in more detail in the appendix, where we place them in the context of appropriate models. For both ordered triangular disk packings and disordered pentagonal packings, when the applied force is below about 0.5 N, there is a reasonable linearity within the error bars. In order to optimize the signal to noise ratio, yet avoid nonlinear effects, we usually chose a working force close to the upper bound of this linear region.

3 Experimental results

In this section, we describe four classes of experiments that address various factors affecting the force propagation in granular systems, including disorder, packing structure, friction, direction of applied forces, and textures.

3.1 Role of packing disorder: Responses of bidisperse systems

As noted, disorder at particle contacts may arise from at least two sources. One is the presence of geometrical disorder in the packing. The other is the random disorder in the contact forces, due for instance, to frictional indeterminacy. We first consider the effects of geometrical disorder on the packing.

The first way that we did so was by determining the force response for bidisperse systems with varying amounts of packing disorder. We modified the amount of disorder in a controlled way as follows: We prepared each sample by mixing about 500 small and 500 large disks in a container, so that $n_1 \simeq n_2 \sim 0.5$. We then randomly chose one particle to add to the upper surface of

the sample until the full amount of particles was in place. The exact values of n_1 and n_2 were determined later from images showing particle configurations using particle identification software mentioned above. The experiments on bidisperse disks were all performed in a nearly vertical plane[4].

It is important to characterize the amount of disorder in the samples. To this end, we have pursued two approaches. The first method involves a parameterization of the width of the disk radius distribution $w(a)$ through the parameter $\mathcal{A} = \langle a \rangle^2 / \langle a^2 \rangle$, as proposed by Luding et al.[4,32] This parameter has proved useful in characterizing the bidispersity of granular systems in the kinetic regime[32]. For our purposes, it is also useful, because it provides a relatively precise way to label bidisperse systems. Specifically, the moments of the distribution $\langle a^m \rangle$ are given by $\langle a^m \rangle = \int w(a) a^m da / \int w(a) da$. $\mathcal{A} = 1$ corresponds to perfect order in a monodisperse situation, and the deviation from unity is proportional to the degree of poly-dispersity or disorder in the system. In a bidisperse system, with respective radii of smaller and larger particles a_1 and a_2 , and corresponding particle numbers N_1 and N_2 , the parameter \mathcal{A} is:

$$\mathcal{A} = \frac{\langle a \rangle^2}{\langle a^2 \rangle} = \frac{[n_1 + (1 - n_1)/R]^2}{n_1 + (1 - n_1)/R^2}. \quad (6)$$

Here, the size ratio is $R = a_1/a_2$, the number fractions are $n_i = N_i/N$ ($i=1, 2$) and the total number of particles is $N = N_1 + N_2$.

Besides the $\mathcal{A} = 1$ case for ordered monodisperse packing, we have used disks with 3 different diameters (0.597 cm, 0.744 cm and 0.876 cm) and obtained bidisperse systems with three different \mathcal{A} values, i.e. $\mathcal{A} = 0.993, 0.988$ and 0.965, as shown in Table 1.

<i>System Type</i>	<i>Disk Diameters</i>	<i>R</i>	<i>n₁</i>	<i>A</i>
monodisperse	0.744 cm	/	/	1
bidisperse 1	0.744, 0.876 cm	0.849	0.590	0.993
bidisperse 2	0.597, 0.744 cm	0.802	0.550	0.988
bidisperse 3	0.597, 0.876 cm	0.682	0.520	0.965

Table 1: Experimental control parameters for the ordered monodisperse system and three bidisperse systems, where R is the size ratio between small and large disks, n_1 the number fraction of the small disk, and \mathcal{A} the disorder parameter.

An alternative method to quantify the disorder of the system is to calculate the particle-particle positional autocorrelation function or radial distribution

function. The autocorrelation function is defined as [32],

$$g(r) = \frac{2A}{N(N-1)} \frac{1}{A_r} \sum_{i=1}^N \sum_{j=1}^{i-1} \theta(r_{ij} - r) \theta(r + \Delta r - r_{ij}), \quad (7)$$

where A is the area of the system, N the number of particles, $A_r = \pi(2r + \Delta r)\Delta r$ the area of a ring between r to $r + \Delta r$, and r_{ij} the distance between particle i and j . The two θ functions select all particle pairs with distances between r and $r + \Delta r$. For bidisperse systems, we calculate the autocorrelation function between the same species and between different species. When calculating the autocorrelation function for different species, the weight $N(N-1)/2$ in the above equation must be changed to $N_1 N_2$ and the indices i and j run from 1 to N_1 and N_2 respectively, in order to account for all pairs of different kinds.

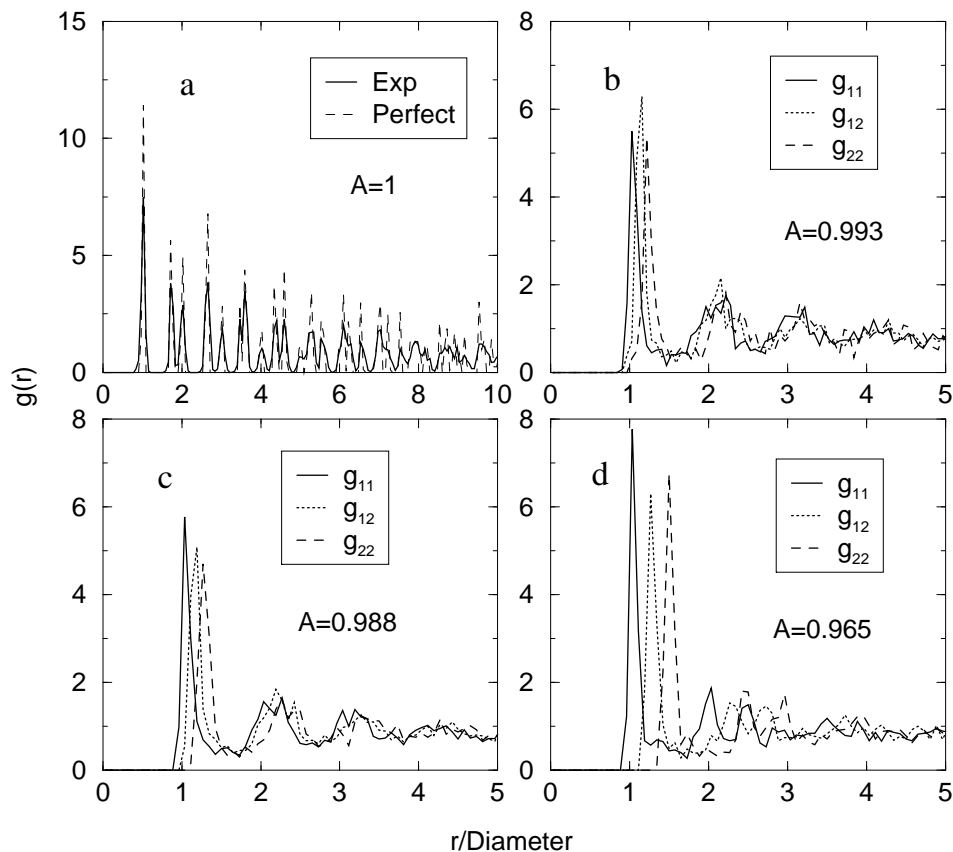


Fig. 6. Particle-particle autocorrelation functions for a) hexagonally packed monodisperse disks, b), c) and d) three bidisperse systems with b) $\mathcal{A} = 0.993$, c) $\mathcal{A} = 0.988$ and d) $\mathcal{A} = 0.965$, respectively. Distances are normalized by the diameter of the smaller particles in each system. In a), the dashed line is calculated from a perfect triangular lattice of comparable size to the experiment, and the solid line is from the experiments. In b), c) and d), g_{11} and g_{22} are correlation functions for the same species of particles and g_{12} are for different species. (see Table I.)

In Fig. 6, we show correlation functions for the monodisperse and three bidisperse disk systems that we have investigated. In Fig. 6a, we contrast the correlation functions calculated from an ideal triangular disk lattice and from an experimentally obtained triangular lattice of monodisperse disks. In the latter case, the broadening of the peaks indicates some irregularity in the packing. However, both correlation functions show a long range order with peaks at $1, \sqrt{3}, 2, \dots$, as expected for a triangular lattice. The decay in the correlation functions is due to the finite size of the system, and has a characteristic length of ~ 8 particle diameters. In Fig. 6b, c and d, we show experimental correlation functions between the same species and between different disk species for bidisperse systems. In contrast to the monodisperse case, we see that over a distance of several disk diameters, the correlations of bidisperse systems decrease very quickly to the background value of 1, and the peaks corresponding to the second and third coordination shell broaden and merge with each other, indicating increasing disorder as the control parameter \mathcal{A} decreases. The correlation lengths, L , for bidisperse systems are 3.86, 3.83 and 3.72, measured in disk diameters, for systems of $\mathcal{A} = 0.993, 0.988$ and 0.965 , respectively, which are calculated according to $L^2 = \int r^2 g(r) d\vec{r} / \int g(r) d\vec{r}$ [33]. Interestingly, the correlation function changes only slightly for these various packings, even though the measured response changes significantly.

We now turn to the experimental results for bidisperse arrays. By increasing the amount of disorder in the system, we observed responses that change from a two-peak structure to a response very similar to that of our most disordered system, namely a system of pentagons. In Fig. 7, we give a greyscale representation of the average response to a point force for the three bidisperse systems with $\mathcal{A} = 0.993, 0.988$ and 0.965 . In Fig. 8, we present the same results by showing the response along a series of horizontal lines at a number of depths, z , measured from the upper surface. For the largest \mathcal{A} , $\mathcal{A} = 0.993$,

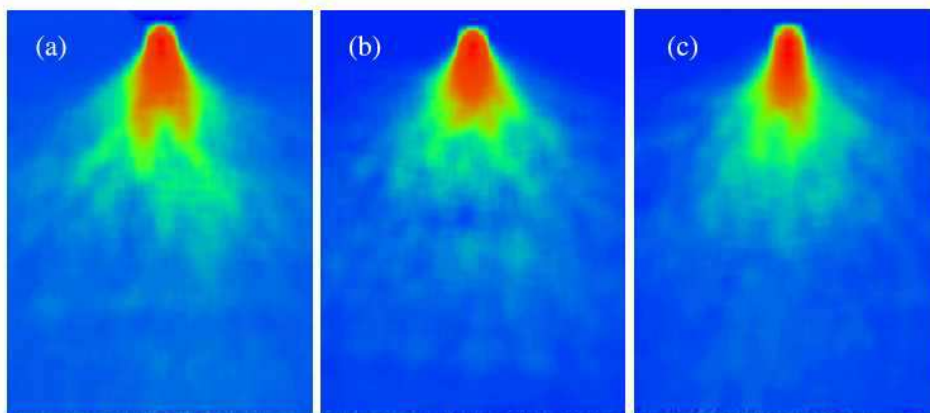


Fig. 7. Mean response for 50 trials of a 50 g point force for bidisperse systems of disks with different amounts of disorder, (a) $\mathcal{A} = 0.993$ (b) $\mathcal{A} = 0.988$ and (c) $\mathcal{A} = 0.965$. The size of each image is 300×400 pixels (about 18.0×13.5 cm).

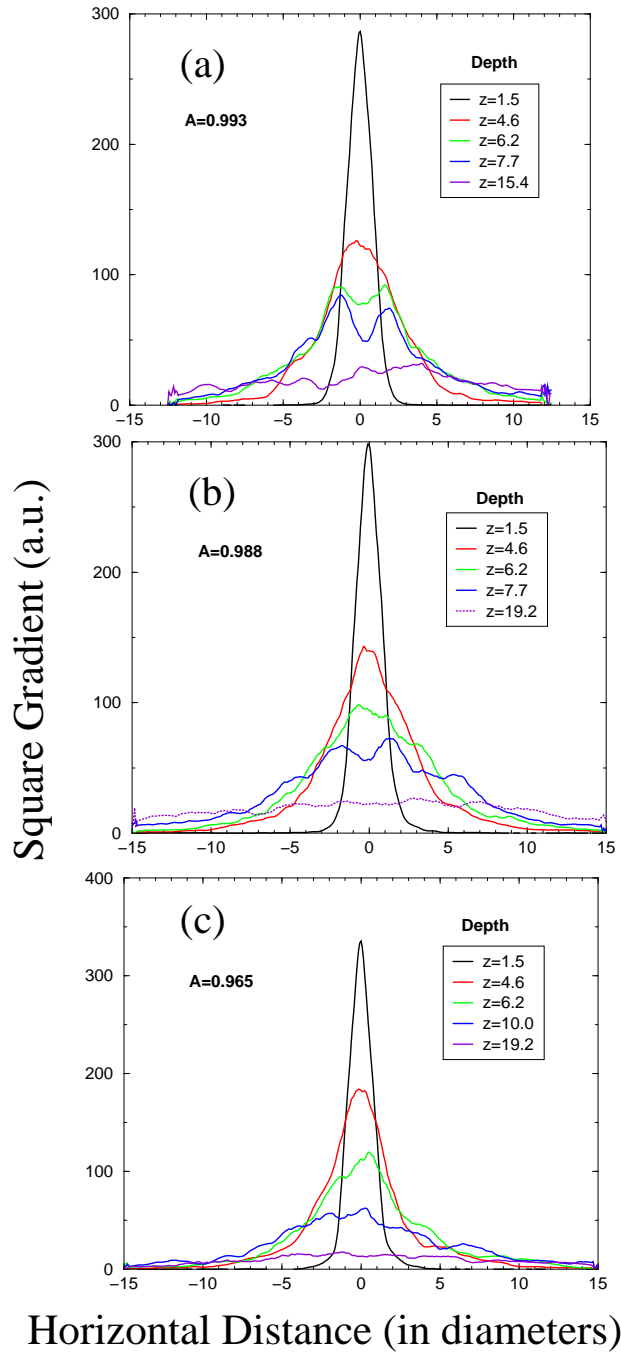


Fig. 8. Photoelastic response, G^2 , to a point force vs. horizontal distance x at various depths z from the source for bidisperse disk systems with a) $\mathcal{A} = 0.993$, b) $\mathcal{A} = 0.988$ and c) $\mathcal{A} = 0.965$, respectively. The horizontal distance and depth in the plots are in units of the smallest relevant disk diameters. The diameters of three different sized disks are 0.597 cm, 0.744 cm and 0.806 cm.

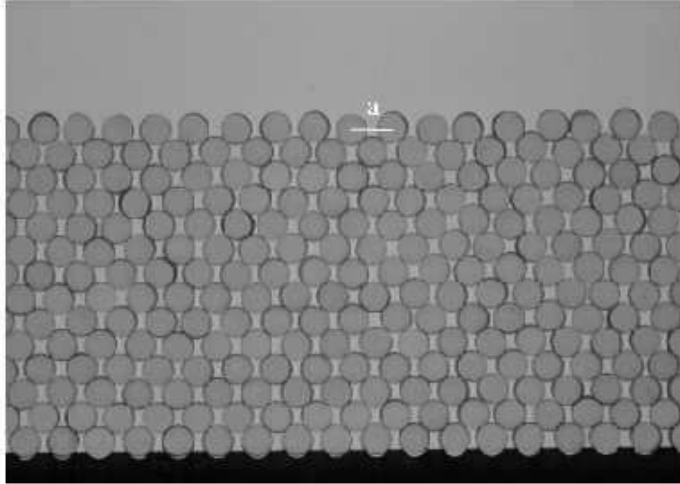


Fig. 9. A rectangular packing of disks with a horizontal lattice constant $a=1.27d$, where d is the disk diameter.

Fig. 7a and Fig. 8a show responses with two-peak features that resemble the response structure for ordered monodisperse disks. However, with decreasing \mathcal{A} , this feature becomes progressively weaker. In Fig. 7c and Fig. 8c, it has completely disappeared, and the response is similar to that of system of pentagonal particles[4] (See also Figs 17 and 18 below). The change from a two-peak to a one-peak structure presents clear evidence of the important role of disorder in force responses.

3.2 Response for rectangular lattices of disks

In the experiments of this subsection, we further consider how packing structure and friction affect the average responses for rectangular lattices. The use of rectangular lattices tends to reduce the randomness of forces at contacts, since all contacts are now essential for stability of the packing. That is, the number of contacts between disks is minimal and the contact network is well defined in the sense that the force at every contact is nonzero. We emphasize, however, that randomness in contact forces still exists, due to friction.

A typical rectangular monodisperse packing is shown in Fig. 9. To construct this packing, disks on the bottom layer were supported by a template consisting of equally spaced grooves with a center-to-center spacing of 1.27 disk diameters. The system size was ~ 85 particles wide and ~ 15 particles high. Since a rectangular lattice has less contacts than a triangular lattice, it is also less stable than a triangular lattice. Consequently, it was more difficult to build tall layers, and once built, a layer could not support as large forces as in the case of triangular packings. Therefore, in this set of experiments, we

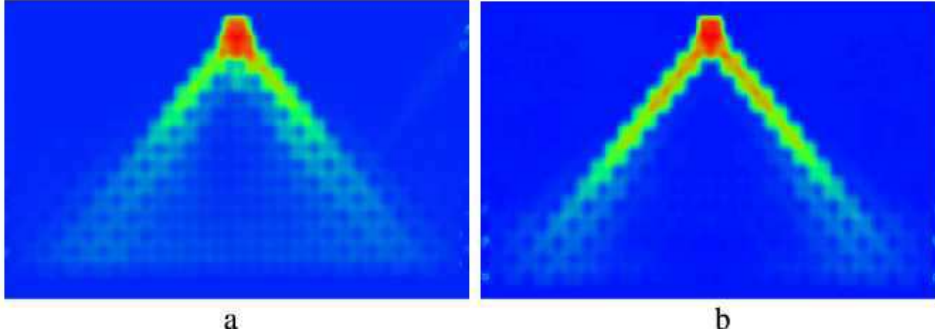


Fig. 10. Mean response for 50 trials of a 20 g point force for rectangular packings of disks: a) relatively frictional disks with a coefficient of friction, μ , close to 0.94, and b) less frictional (Teflon wrapped) particles with $\mu = 0.48$.

used a 20 gram force for the probe.

We note that the naturally occurring surfaces of the disks were relatively frictional, with a static friction coefficient μ close to 0.94. We estimated μ by placing two disks (glued together side-by-side so that they could not roll) on a slope of same material from which the disks are made, tilting the slope and then recording the angle when the particles start to slip. In separate experiments, we wrapped each disk with Teflon tape, thus reducing the friction coefficients to about $\mu = 0.48$. This allowed us to investigate the role of disorder associated with friction in the force response.

In Fig. 10a-b, we show the grey-scale average response pictures for the rectangular lattice systems with large and small friction coefficients, respectively. In Fig. 11, we show quantitative data at several depths for both systems. In both cases, the responses propagate along the lattice directions. The measured value of the angle between the two propagation directions is $\sim 79^\circ$, which corresponds well with the rectangular lattice structure. This is qualitatively similar to the results for a triangular lattice[4], where the angle between the two preferred directions was 60° . For both the higher friction rectangular packing and the hexagonal packing, the peaks in the response broadened relatively rapidly with depth. When the friction was decreased (Teflon wrapped particles) the peaks remained significantly sharper with depth, as shown in Fig. 12. Here, the width w is obtained by fitting a Gaussian curve $F = F_0 e^{-\frac{(x-x_0)^2}{2w^2}}$ to each peak at a given depth. Widths extracted by other means, for example, measuring the width at half maximum height, give similar results. Note that for our usual processing, in which we coarse-grain at the scale of one particle diameter, the smallest peak width is one particle diameter, as seen in the left part of Fig. 12. It is interesting in this case to examine the width of the peaks for the data without coarse graining, as shown in the right side of the figure. These data suggest that in a perfectly ordered and frictionless system, the force response would be perfectly sharp force chains.

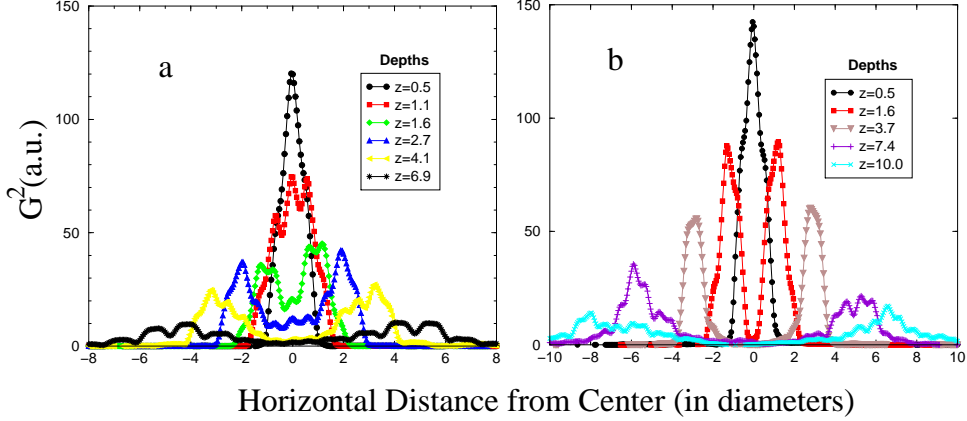


Fig. 11. Photoelastic response G^2 to a point force, vs. horizontal distance, x , at various depths, z , from the source for rectangular packings of disks with different coefficients of friction: a) $\mu = 0.94$, and b) $\mu = 0.48$.

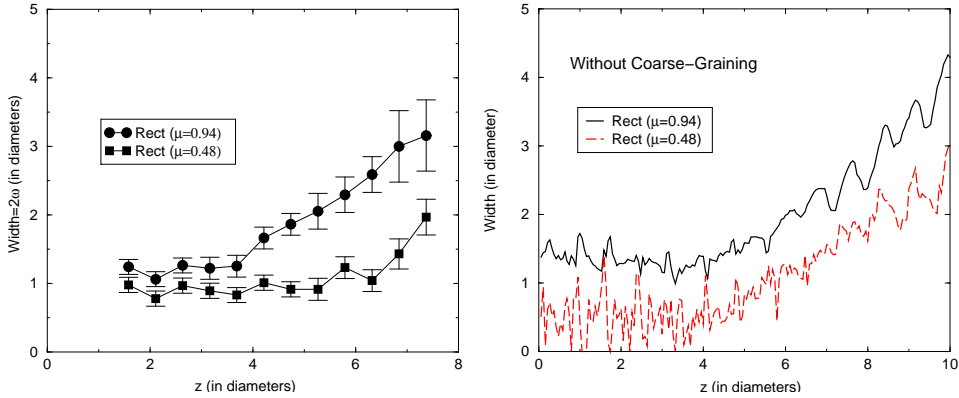


Fig. 12. Width of peaks v.s. depth for rectangular packings of disks with different coefficients of friction. Data on the left show results with the usual coarse-graining average over one diameter. Data on the right is for the same measurements but without coarse graining.

3.3 Comparison to Models

It is useful to compare the observations on bidisperse and rectangular packings to the predictions of Claudin et al[22]. In the case of weak disorder, these authors predict a Convection-Diffusion equation, as discussed in the Appendix. This equation is characterized by a propagation speed, c , that determines the opening angle of the two-peak response, and by a diffusivity, D , that determines the rate at which the peaks broaden with depth. These authors predict that D grows and c decreases as the disorder increases. In order to make contact with this model, we determined c and D by finding nonlinear least-squares fits of the mean responses for a given type of system at all depths to the CD equation simultaneously. At large depths, the data approach the noise floor, and it is not possible to resolve the two-peak structure. Accordingly, we fit only

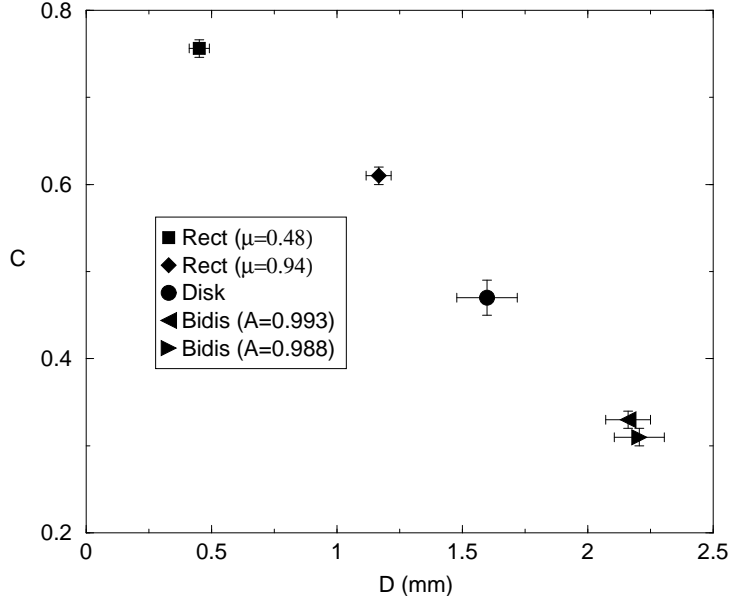


Fig. 13. The coefficients of c and D extracted by fitting the mean responses from different systems to the CD equation. Each point in the graph corresponds to a different system. See the text for more detail.

the regions from about 2 to 10 grains deep. In Fig. 13, we show the resulting coefficients c and D extracted from the disk data and from several other data sets discussed below. The error bars in Fig. 13 represent a 95% confidence interval for each parameter. In Fig. 14, we show an example of such fits. Fig. 14a shows a perspective 3D plot of the mean response from experiments for a rectangular packing of disks with a frictional coefficient $\mu = 0.48$, and Fig. 14b shows the least-squares fit of the experimental data to the CD equation. In Fig. 14c, we compare for various depths the profiles of the experimental data (symbols) and the fits to the CD equation (solid lines). One can quantify the goodness of a nonlinear fit by calculating a value R^2 , a so-called coefficient of determination[34]. The closer that R^2 is to 1, the better the fit is. In our fits, the R^2 values are in the range of $0.8 \sim 0.9$. An excellent fit corresponds to values of R^2 only slightly less than 1. However, considering the complexity of the data and fits, we believe the data are described reasonably, although not exactly, by this model.

In total, Fig. 13 shows fit results for c and D of the CD equation for five different systems. These systems include two rectangular lattices with friction coefficients $\mu = 0.48$ and $\mu = 0.94$, a hexagonal packing of monodisperse disks, and the two randomly packing bidisperse disk systems with $\mathcal{A} = 0.993$ and 0.988 . This figure suggests that, as the disorder in the system increases, the coefficient c decreases and the coefficient D increases.

One possible way to distinguish between predictions of Bouchaud et al.[6,7] and anisotropic elasticity models[8] is by determining how the width of each

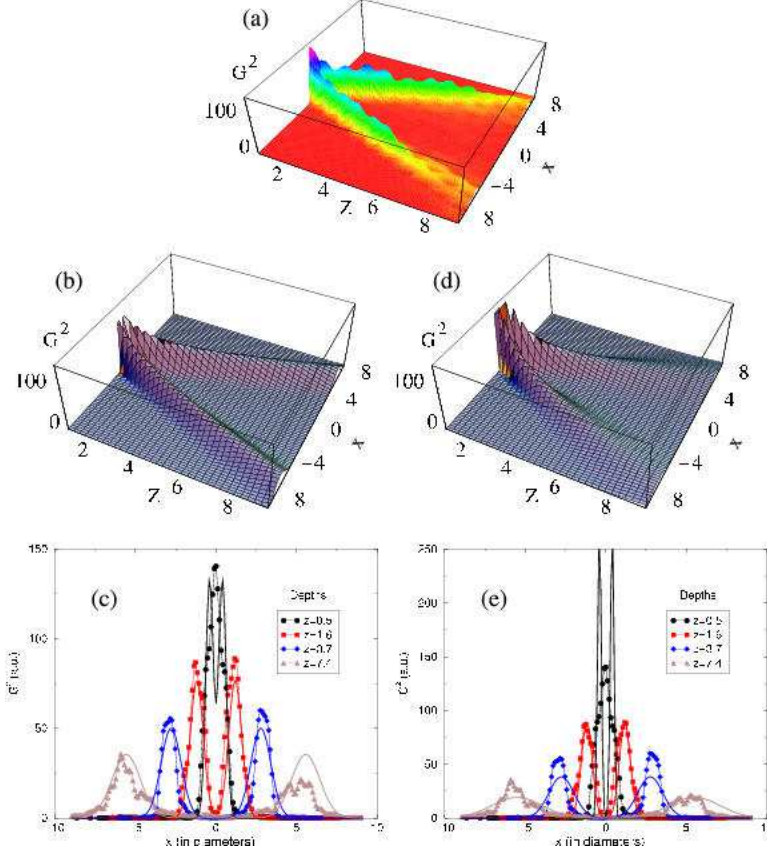


Fig. 14. Comparison of nonlinear least-squares fits to the CD equation and the CW equation for a rectangular packing of disks with a frictional coefficient $\mu = 0.48$. a) a perspective 3D plot of the experimental response, b) a 3D plot of the least-squares fit to the CD equation, and c) comparison of profiles of the experimental data and the fitting data at different depths, where the symbols are experimental data and solid lines are fits. d) and e) are similar to b) and c), but for the CW equation. Here, x and z are measured in disk diameters.

peak changes with depth. For the former, one expects a width that grows with square-root of depth, and for the latter, a width that grows linearly with depth[7]. Note that the width for the data of Fig. 12 is nearly constant at roughly a particle diameter for these data, until a depth of about four particle diameters, whereafter it grows with depth. The data for the width vs. depth then suggest more of a linear variation than a square-root variation, particularly in the data of Fig. 12 that have not been coarse-grained. At this time, however, based on our data, it does not seem possible to distinguish between these two models.

Nevertheless, it would be useful to have a simple functional form, similar to the solution of the CD equation (see Appendix) to which we could fit complete data sets. Although at this time we are not aware of a specific (simple) functional form for force transmission in an elastic system with disorder, we have fitted the results to a functional form that has a number of the proper-

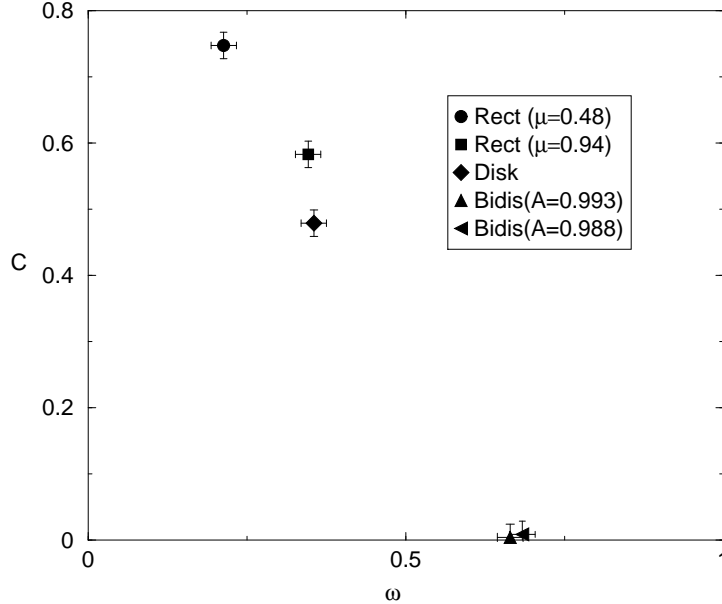


Fig. 15. The coefficients of c and ω extracted by fitting the mean responses from different systems to the CW equation. Each point in the graph corresponds to a different system. See the text for more detail.

ties that we expect from such a solution. These include preferred propagation directions, and a width that increases linearly with distance from the source. The functional form that we have used, denoted as the CW equation, has these properties, as discussed in the Appendix. This function consists of two gaussians that propagate along the direction defined by a velocity, c , and that widen linearly with depth. That is, we replace the width function, $W \propto z^{1/2}$ in the CD model with $W = \omega z$, where ω is a system-dependent constant. The two parameters in the CW equation are the propagation speed c and ω . These play similar roles to c and D in the CD equation. In Fig. 14d and e, we show a sample fit to the CW equation. In Fig. 15, we show the fitted coefficients c and ω , where the quality of the fits is comparable to what was obtained with the CD equation. As the disorder in the system increases, the coefficient c decreases and the coefficient ω increases, an effect that is similar to the results in Fig. 13. For the two-peak behavior shown in Fig. 13 and 15, the values of c correspond rather well, within uncertainties, to the value of the lattice directions assumed by the packing geometry as in Fig. 10. This is consistent with the point of view of anisotropic elasticity models[8].

3.4 Non-normal force responses

We consider the vector character of force propagation in this section, namely the response to forces applied at arbitrary angles to the surface. We first consider the response to a non-normal force in a disordered system, one consisting

of pentagonal particles. We then consider the corresponding problem for an ordered system, in this case monodisperse disks in a triangular packing.

As in the previous measurements, particles were placed in a vertical plane, and forces were applied on a single grain at an angle θ with respect to the horizontal direction. Specifically, a force of 50g was applied to the surface at angles, 90° , 60° , 45° and 30° with respect to the horizontal for pentagons and at 90° , 75° , 60° , 45° , 30° and 15° with respect to the horizontal for a hexagonal packing of disks. The line of force was chosen so that, as much as possible, it passed through the center of gravity of the grain. In other respects, the procedure and analysis were the same way as we described previously.

For the case of a disordered system, such as a packing of pentagonal particles, we have shown[4], as a special case, that an applied normal force at a boundary produces a response that resembles that of an elastic solid. As a point of reference, when a force is applied to an elastic plate of thickness t at an arbitrary angle θ with respect to the horizontal direction, as depicted in Fig. 16, the stress tensor components are[35]:

$$\sigma_{rr} = \frac{2Ft}{\pi r} \cos\phi, \quad \sigma_{r\phi} = \sigma_{\phi\phi} = 0, \quad (8)$$

where the angle ϕ is measured from the direction of the applied force, r is the distance from the point under consideration to the point of contact. When converted to Cartesian coordinates, where the z -axis is aligned with the applied force, the stress components have a simple scaling form, as seen for instance in the stress component

$$\sigma_{zz}(x, z) = \frac{2F}{z\pi} \frac{1}{[(x/z)^2 + 1]^2}. \quad (9)$$

Note that $z\sigma_{zz}(x, z)$ depends only on the ratio of x to the depth, z . A similar conclusion applies to all components of the stress tensor.

The dashed circles shown in Fig. 16 represent loci of equal stress, σ_{rr} . For the case of an elastic plate, when the direction of applied force changes, these equal-stress lines remain the same with respect to the direction of the force, except for those points that lie outside of the material.

In Fig. 17, we show the grey-scale representation of the average responses for pentagonal particles. In general, the force responses are centered along the direction of the applied forces and, particularly for larger angles, they are similar to a rotated version of the response when a normal force is applied. This is more evident in Fig. 18. To obtain this figure, we first rotated the reference frame so that the z -axis corresponds to the direction of the applied force. From

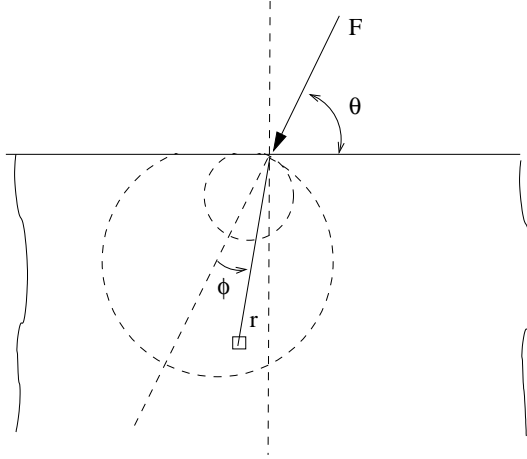


Fig. 16. Schematic drawing of a force applied to the surface of an elastic semi-infinite plate at an angle θ with respect to the horizontal. Here, r is the distance from the point of contact, and ϕ is the angle from the direction of the force, measured counter-clock-wise.

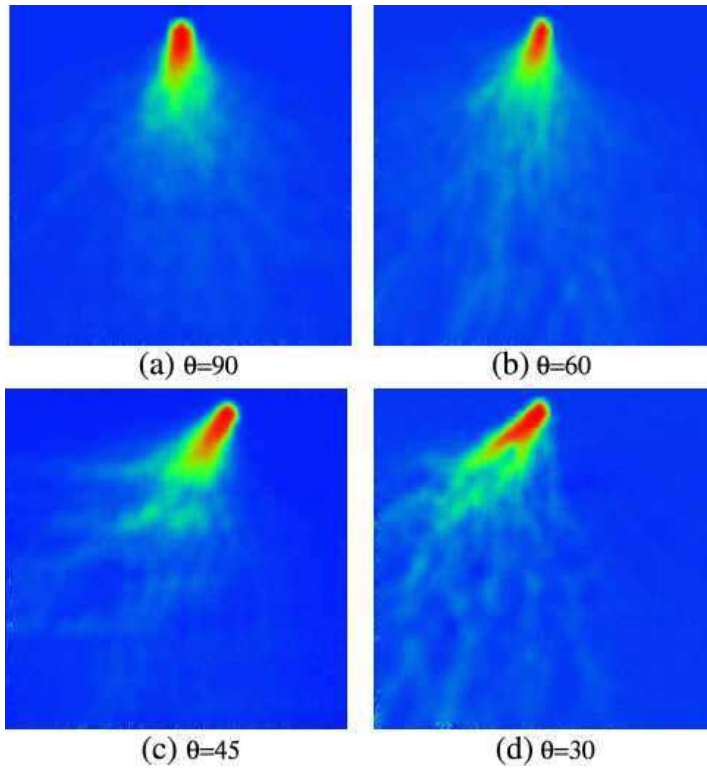


Fig. 17. Non-normal force responses for a system of pentagonal particles. A force of 0.5N was applied on the surface of the sample. The force directions are: (a). 90° , (b) 60° , (c) 45° and (d) 30° , with respect to the horizontal.

the data, we computed the force responses along a series of horizontal lines at depths, z , in the rotated coordinate system. We then rescaled these responses as follows: we normalized the x coordinate by the value of the depth, z in the

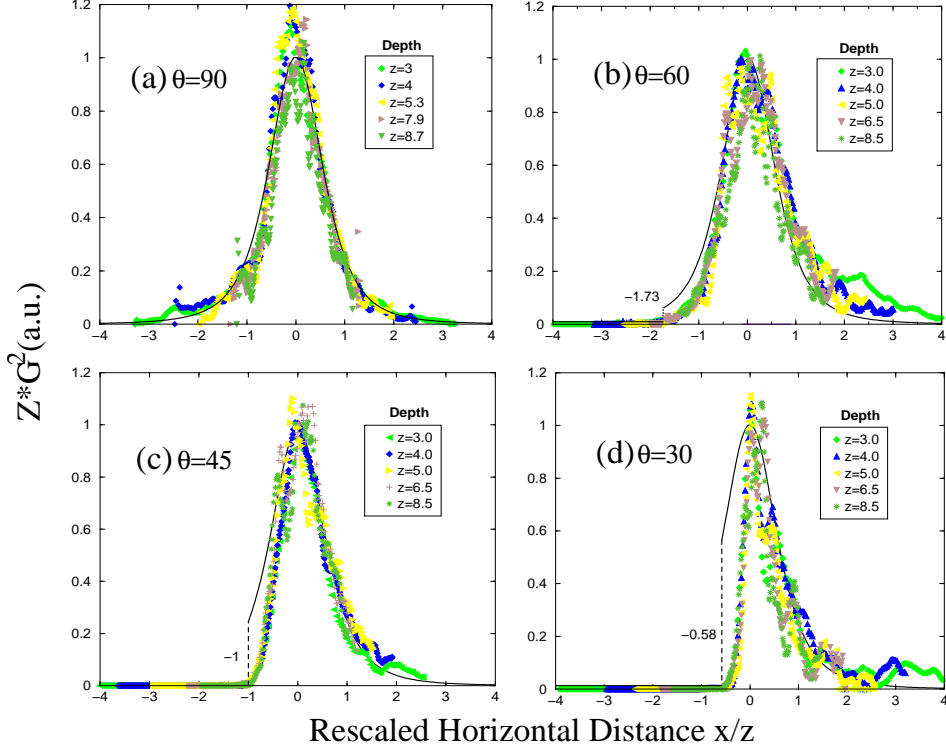


Fig. 18. Rescaled mean force responses in a system of pentagonal particles for non-normal forces applied at various angles: (a) 90° , (b) 60° , (c) 45° and (d) 30° . To obtain this figure, we first rotate the coordinate axes for the response so that the vertical axis is along the direction of the applied force, and we then obtain the force responses along a series of horizontal lines at depths, z , measured from the source. We then rescale these responses as follows: 1) we normalize the x coordinate by the depth, z in the rotated frame, and 2) we multiply the stresses by z in the rotated frame. Solid lines are the semi-infinite elastic plate solution.

rotated frame, and we multiplied the stresses by z in the rotated frame. For comparison, we plot the elastic plate solutions based on Eq. 8 in these figures. Fig. 18a is a confirmation that the response to a normal force is consistent with that of a 2D elastic material, i.e., the widths of response vary linearly with the depth. Fig. 18b, c and d show that the mean responses to forces at other angles in a pentagonal system have the scaling property of an elastic medium. However, the response function on the side towards which the force is directed clearly deviates from the elastic solution. The deviations from the elastic solution on this side in b, c and d may be attributable to the fact that there are no tensile forces in a granular material. Thus, this figure suggests that on the side opposite to the direction of the applied force contacts may open, a process that has no analogue in the formalism of a conventional elastic solid. It seems likely, however, that this process is still reversible, since there was no observable rearrangement of the particles, once the applied force was removed.

Next, we consider the response to a non-normal force on the boundary of

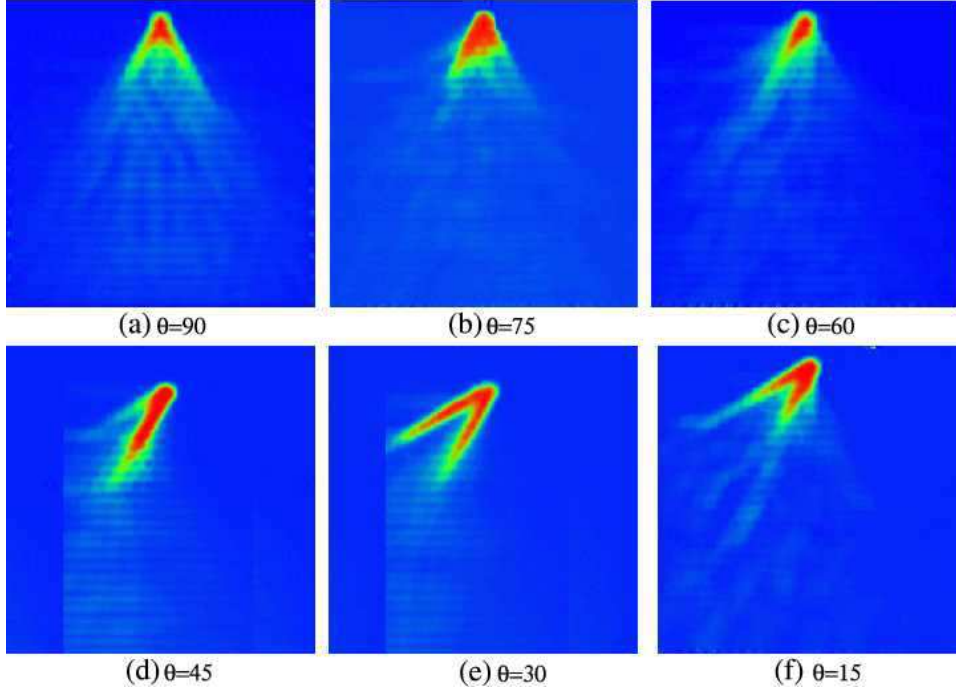


Fig. 19. Responses for a non-normal force applied to a hexagonal packing of monodisperse disks. A force of 0.5N was applied on the surface of the sample. The force directions are: (a) 90° , (b) 75° , (c) 60° , (d) 45° , (e) 30° and (e) 15° , and all angles are with respect to the horizontal.

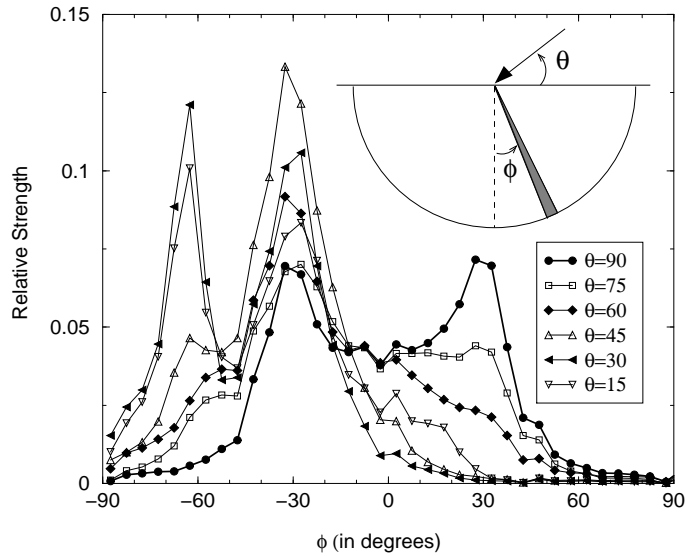


Fig. 20. Relative strength of the response in a given direction, ϕ , when a force is applied at an angle, θ . The definition of ϕ is illustrated in the inset.

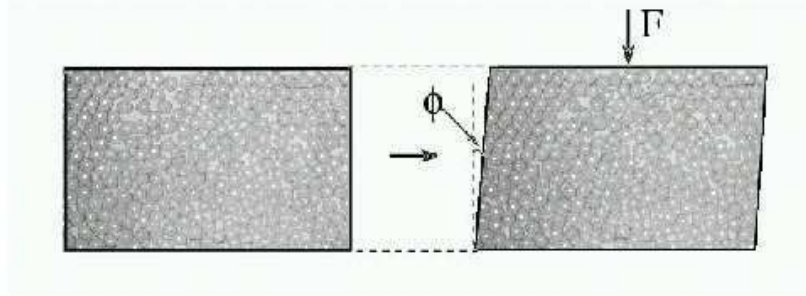
a triangular packing of monodisperse disks. In Fig. 19, we show the grey-level average response pictures for systems where a force of 50g was applied to the surface at angles: 90° , 75° , 60° , 45° , 30° and 15° , with respect to the

horizontal. For the $\theta = 90^\circ$ case, the mean response is along the two lattice directions closest to the applied force direction, and left-right symmetry is preserved. For the $\theta = 75^\circ$ case, the left-right symmetry is broken, but the response still involves the same two lattice directions. Specifically, the response along the left lattice direction (i.e. most closely aligned along the applied force direction) is strong, and the response along the right lattice direction is relatively weak. For the $\theta = 60^\circ$ case, where the force is applied along only one of the principal lattice directions, we see that the response is only along that direction. For each of the $\theta = 45^\circ, 30^\circ$ and 15° cases, part of the average responses is aligned along the left principal lattice direction, and part is aligned along a new direction that is $\sim 62.5^\circ$ clock-wise from the vertical direction. This is illustrated more quantitatively in Fig. 20. To obtain this figure, we first partitioned the responses of Fig. 19 into small angular bins, 5° in width, and we then calculated the integral over the radial direction of the responses in those bins. Thus, these curves show the total strength of the response in a given direction. The two principal lattice directions are -30° and $+30^\circ$. The other direction, $\phi = -62.5$, is associated with the next-nearest neighbor lattice direction which is aligned most closely with the direction of the applied force. It is interesting to note that propagation along this direction involves a more complex process than that involved with particles that are aligned along the principal lattice directions. It seems likely that friction plays an important role in this process.

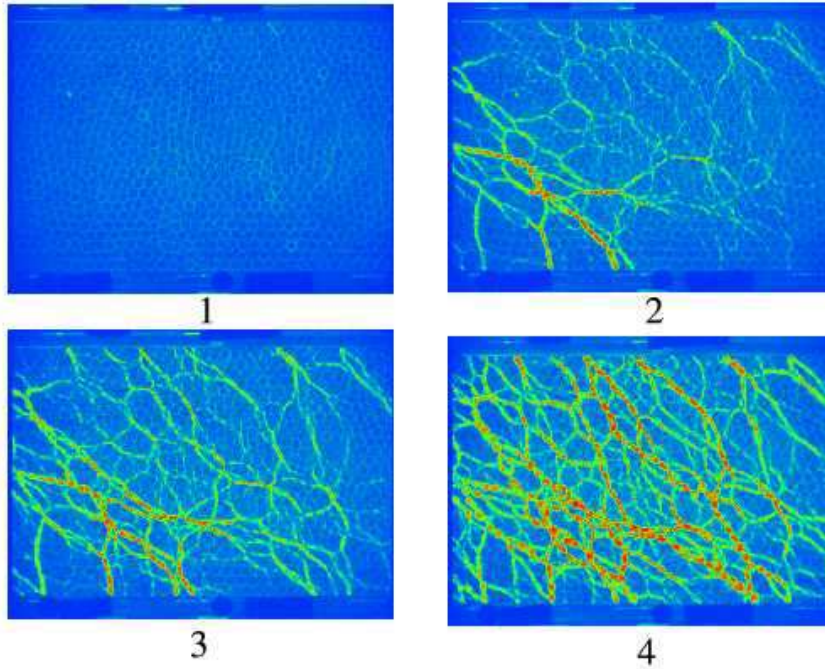
3.5 Responses of a system with shear deformation

In this final section of experiments, we consider the characterization of stress chain orientation and length in a system that has been subjected to a modest amount of uniform shear, and how such systems respond to applied external forces. In essence, this is a probe of the nature of anisotropic texture.

We created an anisotropic texture by applying nearly uniform simple shear. To do so, we constructed an experimental setup that is sketched in Fig. 21(a). The particles, in this case pentagons, rested on a flat horizontal surface consisting of Plexiglas, and they were confined by Plexiglas walls. Two parallel boundaries were hinged at their lower corners so that it was possible to shear the system. The other two boundaries remained parallel during the shearing process. One of these latter boundaries remained fixed relative to the Plexiglas bottom plate, and the other, which was opposite the hinges, was guided so as to keep constant the distance between the opposite parallel boundary. Hence the available area to the particles remained constant. The system size was about $\sim 47 \text{ cm} \times \sim 22 \text{ cm}$. We applied controlled amounts of shear to this system by slowly displacing the upper left corner of the boundary by a measured amount. For this experiment, we used 1167 pentagonal particles that



(a)



(b)

Fig. 21. (a) Schematics of the 2D shearing cell with real images of the pentagonal particles overlaid. The small black dots on each particle denote their centers of mass. (b). A series of photoelastic images showing stress chain patterns for different amounts of shear deformation. The shear deformation increases with the image number: $\phi=0$, 2.4° , 3.2° and 4.8° for image 1, 2, 3 and 4, respectively.

were ~ 6.3 mm on an edge. The packing fraction was 0.795.

The experimental procedure was the following: (1) the left edge was pushed continuously until it reached a given angle, ϕ , with respect to the normal direction. A typical series of stress patterns as ϕ was increased is shown in Fig. 21(b). (2) Then a small local force perpendicular to the top edge was applied on a particle at the top boundary and the response image was recorded. (3) The force was removed and the background image was recorded. (4) We then followed the general image processing procedure as described above to obtain the mean response. By taking images without polarizers, we were able

to obtain particle positions, as shown in Fig. 21(a), and thus, we were able to calculate the texture tensor. We also characterized the orientation and length of stress chains which are typified by Fig. 21(b), through the use of two point spatial correlation functions for the stress.

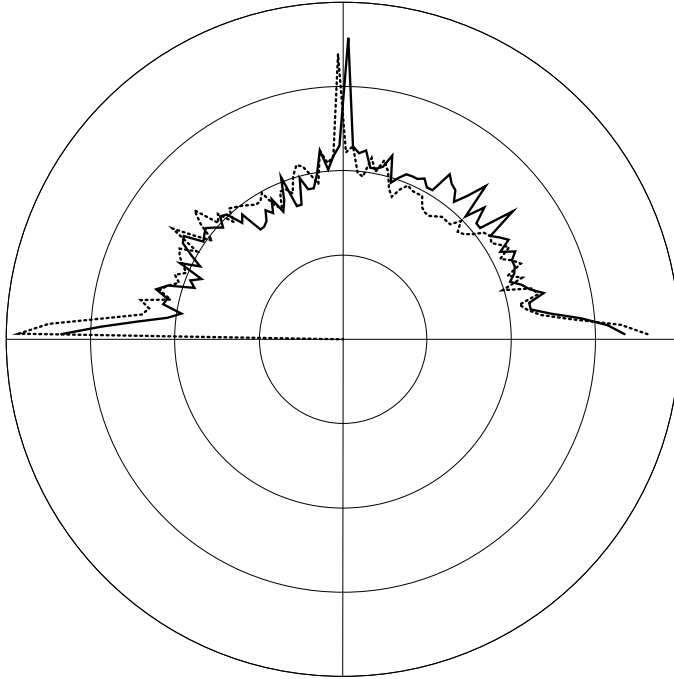


Fig. 22. Comparison of distributions, $\rho(\theta)$, of fabric tensor principal directions before (Dotted line) and after (Solid line) the shear deformation is applied. The distributions are averaged over all the particles and over 50 runs.

We first examine the impact on the texture, characterized by the fabric tensor, as in Eq. 1, due to the shear deformation. Since there can be a range of distances for two pentagons to be in contact, we consider a contact to exist if the distance between centers of two pentagons falls within the interval $[r_{min}, r_{max}]$, where r_{min} and r_{max} correspond to the minimal and maximal distance between centers of two pentagons while they are still in contact. Thus, the contacts between pentagons may be overestimated. When the fabric tensor is diagonalized, its major principal direction, θ , gives the direction, along which the particles have, on average, the largest number of contacts. A comparison of the distributions of these principal directions, $\rho(\theta)$, for all particles before and after the application of a shear deformation to the system, provides a quantitative measure of how much the geometric contact structure has changed. In Fig. 22, we show such a comparison. The dotted line shows the distribution before the shear deformation is applied and the solid line is after the shear deformation. These data are averaged over all the particles and over 50 runs. We observe that there are more contacts along the horizontal and vertical directions than any other directions for both the “before” and “after” cases, which can be explained by the fact that the particles align with the boundaries. In the “after” case, the distribution is slightly skewed from

that of the “before” case. Notably, the change in texture is not nearly as significant as the changes in the stress chains, which we will discuss next. However, caution needs to be taken in interpreting data shown in Fig. 22. Since a relatively small change in the displacement, in the order of microns, is enough to produce a large contact force, those minute structural changes may not be detected in the current experimental measurements using fabric tensors, which has a resolution of about 0.5 mm (1 pixel).

In Fig. 21b, we show the impact on the stress chains caused by applying a small shear deformation. This set of images follows the course of a deformation beginning with $\phi = 0^\circ$ and ending with $\phi = 4.8^\circ$. An obvious result of this deformation is that the stress chains tend to align in a direction that opposes the deformation, but at an angle that greatly exceeds the angular strain. A similar stress chain alignment was observed in 2D Couette shear [36], although in this case the strains were very large. In the present experiments, the stress chain orientation tended to saturate following a small angular deformation, i.e. for $\phi \gtrsim 5^\circ$, the typical stress chain angle did not significantly change. We return to this point below.

An important issue concerns the spatial structure of the stress chains that are generated in response to such a deformation. With images such as those shown in Fig. 21(b)3 and 4, where stress chains are well defined, we can characterize the stress chain orientation and chain length by calculating the spatial auto-correlation $c(\mathbf{r})$ for the stress, i.e. G^2 :

$$c(\mathbf{r}) = c(r, \theta) = \langle G^2(\mathbf{x})G^2(\mathbf{x} + \mathbf{r}) \rangle, \quad (10)$$

where the brackets denote an average over spatial coordinates \mathbf{x} . In this calculation, it is important to retain angular information in $c(r, \theta)$ in order to extract information about the anisotropic features of the system. The actual calculation of the correlation function is performed in wavenumber space using FFT (Fast Fourier Transform) techniques, since the computation in the space domain is cumbersome when the image size is large, e.g. 512×512 pixels.

Fig. 23 shows such a spatial auto-correlation function $c(r, \theta)$ in a perspective 3D plot on the left, and in greyscale on the right. These data are obtained by averaging 50 realizations. Clearly, and perhaps not surprisingly, these images show that correlation along the stress chain directions is much longer range than along the perpendicular direction, even though the stress chain directions span a finite range of angles. The strongest direction for $c(r, \theta)$ is 45° from the vertical. Fig. 24 shows the correlation function evaluated along this direction and the direction perpendicular to it. Along the perpendicular direction, the correlation is almost a δ function, dropping rapidly to a value close to zero over a distance of about 1 grain diameter. However, along the strong direction, the correlation function is consistent with a power law with an exponent of

-0.81, showing long range order over the size of the system.

These data may also shed some light on an apparent conflict between different force measurements by Liu et al.[20] and by Miller et al.[37]. In the first

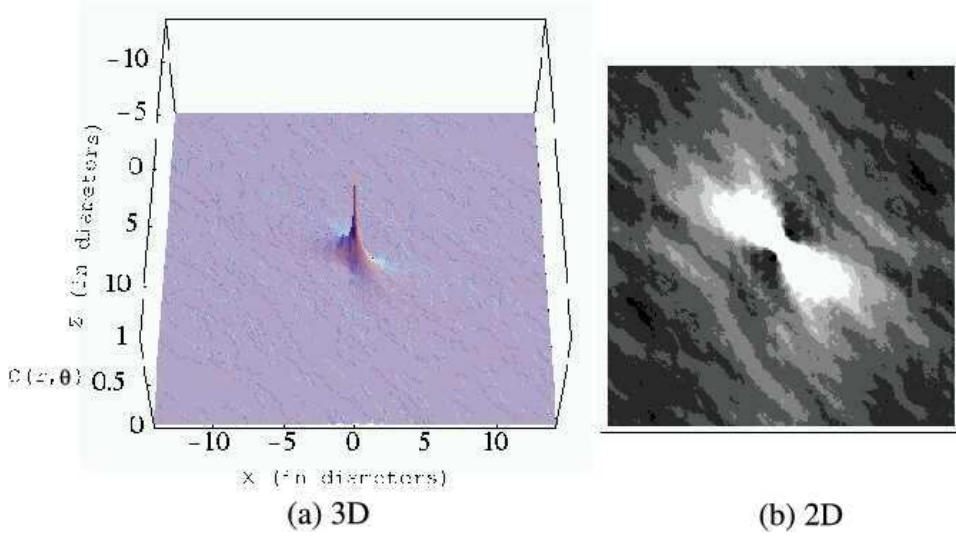


Fig. 23. 3D (a) and 2D (b) representations of the spatial auto-correlation function $c(r, \theta)$ for stresses in a shear cell (as typified by Fig. 21(b)3,4). These data are an average of 50 independent realizations. The image size is 512×512 pixels, cropped from the original image which is 640×480 pixels and padded at the edge with the mean intensity, for computational efficiency. These images show that the correlation along the stress chain direction is much stronger than along the perpendicular direction.

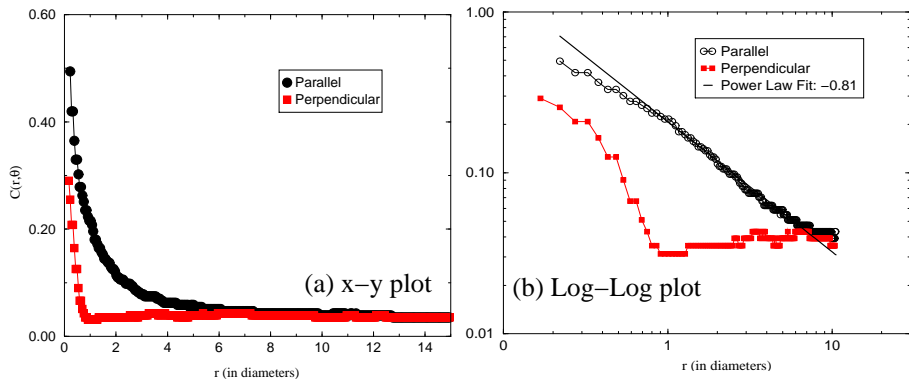


Fig. 24. (a) Spatial auto-correlation function $c(r, \theta = 135)$ (parallel to the stress chain direction) and $c(r, \theta = 45)$ (perpendicular to the stress chain direction). Here, θ is measured from the right horizontal direction. (b) same data shown on double logarithmic scales. The correlation function parallel to the stress chain direction can be fitted with a power law: $c(r, \theta) \sim r^{-\gamma}$, where γ is 0.81, showing a persistent long range order. In the direction transverse to the chains, the correlation function falls to the background value over a length that is roughly one grain size. Note that distances are measured in particle sizes.

set of experiments, a granular system was subject to uniaxial compression, and forces were then measured in a plane that was normal to the direction of compression. No correlations were observed between forces in the plane of the measurement. In the second set of measurements, stresses were measured at the boundaries of a system undergoing plane shear. In this case, the data indicated correlations in the forces. The possible explanation here may be that for the first experiment, the stress chains were normal to the plane of measurement, whereas in the latter, the stress chains were likely tilted relative to the plan of measurement by something like 45° .

The angle 45° seen in the correlation function above, can be understood by noting that for small angles of shearing, ϕ , simple shear can be expressed as a solid-body rotation by $\phi/2$ plus compression along a line oriented at 45° (the strong stress chain direction) and an expansion at 90° to that direction. Thus, the strong asymmetry set up in the stress network is associated with strengthening of contacts due to the compression. It seems likely that this strengthening can occur in the case of angular non-space-filling particles with minimal change in the contacts, and hence in the texture.

Lastly, we consider the impact of anisotropy in the stress chain network on force propagation. When a vertical force was applied, the force tended to propagate along or toward the stress chains. Specifically, on average, a force applied normally to the upper boundary led to a force response whose peak deviated from the vertical direction, as shown in Fig. 25. In Fig. 26a, we give data for the response at different depths for a 4.7° deformation. In Fig. 26b, we plot the same data but we rescale the x coordinates with depth z . In this

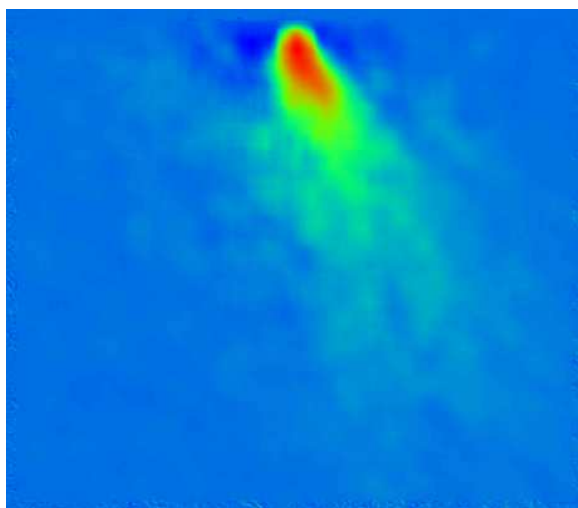


Fig. 25. Mean force response in a pentagonal system that was prepared with a shear deformation of 4.7° . The force is applied normal to the top edge. Note the sheared-induced anisotropic contact network has significantly changed the force propagation direction, in contrast to the response for an isotropic system of pentagons.

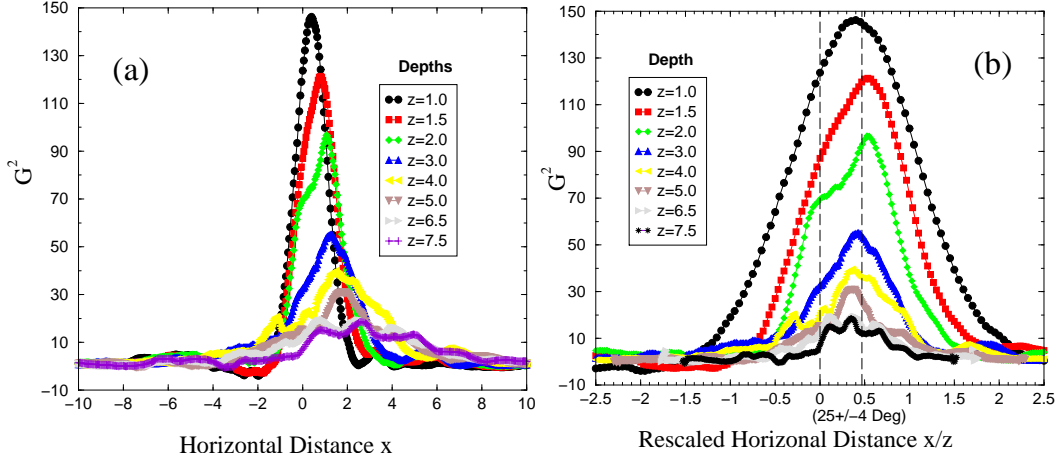


Fig. 26. Quantitative representation of the data from the previous figure for a pentagonal system with shear deformation of 4.7° : (a) The averaged photoelastic response, G^2 , v.s. horizontal distance, x , at various depths z . (b) The same data as (a), but with the x coordinate rescaled with the depth z . In both plots, x and z are measured in grain sizes, where a grain size is about 1 cm.

latter figure, all peaks of the responses at different depths are roughly located around $x/z = 0.5$, which is about $25 \pm 4^\circ$ from the vertical.

4 Summary and conclusions

We have measured the force response of 2D granular systems to local perturbations under various conditions. There are large variations from realization to realization, and we consider ensembles built from many repeated observations under identical conditions. We have obtained ensemble-averaged responses for five types of systems: monodisperse systems packed in an ordered triangular lattice, bidisperse systems with different amount of disorder, monodisperse systems packed in an ordered rectangular lattice, systems with forces applied at an arbitrary angle at the surface, and systems that have been subject to shear deformation, hence with textured/anisotropic features. We find that disorder, packing structure, friction and textures affect the average force response in a granular system significantly. Specifically, we have found that: 1) in ordered triangular packings, normally applied forces propagate along the principal basis vectors of the lattice; 2) in bidisperse systems, when the amount of disorder is increased by adjusting the size and number ratio of large and small disks, the average response to normally applied forces changes from a response with a two-peak feature to a one-peak response; 3) in a rectangular lattice system, forces propagate along the lattice directions and when the friction between particles is decreased, the mean response becomes sharper; 4) when a force of arbitrary direction is applied at the surface of a disordered packing (pentagonal particles) the mean response can be described by an elastic solution; 5)

when a force of arbitrary direction is applied at the surface of an ordered packing (hexagonal packing of disks) the mean response propagates along lattice directions which may include next-nearest-neighbor directions; 6) in a system with shear-induced anisotropy, the stress chains tend to orient along roughly a 45° degree angle so as to strongly resist the additional deformation; 7) in such an anisotropic system, force correlation along the preferred direction is long-range, and the correlation function is a power law with an exponent of -0.81 ; 8) and in such an anisotropic system, the resulting average response to a normal local force tends to propagate along or toward the preferred force direction.

These results help identify the important factors that affect force propagation in granular media and thus raise the need to incorporate these factors into models. The data are inconsistent with the scalar q -model. At this time, it is not possible to distinguish between essentially propagative models by Bouchaud et al. and anisotropic elasticity models as suggested by Goldenberg and Goldhirsch. However, the wave-like propagation seen by Tkachenko and Witten for polydisperse frictionless particles was not seen in these experiments. There are a number of important issues to address in the future. One of these involves improved techniques and tests to help further narrow down the range of prospective models. This might involve examining the role played by the boundaries, which differs between hyperbolic and elliptic systems. In addition, it would clearly be valuable to further develop the photoelastic resolution. Other interesting and related issues concern the force response to distributed loads and the force response when plastic deformations occur. We will address these issue in future work.

Acknowledgements

We appreciate helpful interactions with P. Claudin, S. Luding, C. Goldenberg, I. Goldhirsch, and J. Socolar. The work of GR and EC was supported by PICS-CNRS #563. The work of JG and RPB was supported by the US National Science Foundation under Grant DMR-0137119, and DMS-0204677, and by NASA under Grant NAG3-2372.

A Appendix

This appendix serves two roles. First, it summarizes some important properties of the Convection-Diffusion equation, and of the elastic response function for a semi-infinite solid sheet[35]. In addition, it uses these models to pro-

vide a setting in which to examine the linearity of the response seen in the experiments.

A.1 Summary of the Convection-Diffusion equation properties

Here, we briefly review the two branch Convection-Diffusion equation(CD) adapted from Ref.[22] which is intended to be relevant for weakly disordered systems.

The CD equation is:

$$\mathcal{O}^+ \mathcal{O}^- \sigma_{zz}(x, z) = 0 . \quad (\text{A.1})$$

Here, $\mathcal{O}^\pm = \partial_z - D\partial_{xx} \pm c\partial_x$, x and z are horizontal and downward coordinates, and c and D are two parameters in analogy to a dimensionless velocity and a diffusion coefficient. The solution to this equation for a delta function initial condition, $\sigma_{zz}(x, 0) = F\delta(x, 0)$ is

$$\sigma_{zz}(x, z) = \frac{F}{2} \left(\frac{1}{\sqrt{4\pi Dz}} e^{-\frac{(x-cz)^2}{4Dz}} + \frac{1}{\sqrt{4\pi Dz}} e^{-\frac{(x+cz)^2}{4Dz}} \right) \quad (\text{A.2})$$

where F is the magnitude of the downward delta function stress.

In order to provide an alternative description to the CD equation, we used what we call **CW equation**. Here, the point is to incorporate some of the expected features of an elastic model into a simple fitting function. In a similar spirit to the CD equation, we write

$$\sigma_{zz}(x, z) = \frac{F}{2} \left(\frac{1}{\sqrt{2\pi W}} e^{-\frac{(x-cz)^2}{2W^2}} + \frac{1}{\sqrt{2\pi W}} e^{-\frac{(x+cz)^2}{2W^2}} \right) \quad (\text{A.3})$$

where $W(z)$ is the width of each peak. For the CD model, $W = \sqrt{2Dz}$. If we replace the diffusively increasing width by a linearly increasing width, $W = \omega z$, where ω is a constant, we obtain the CW description:

$$\sigma_{zz}(x, z) = \frac{F}{2} \left(\frac{1}{\sqrt{2\pi\omega z}} e^{-\frac{(x-cz)^2}{2\omega^2 z^2}} + \frac{1}{\sqrt{2\pi\omega z}} e^{-\frac{(x+cz)^2}{2\omega^2 z^2}} \right). \quad (\text{A.4})$$

A.2 Elastic response and tests for linearity in ordered systems

This model provides a convenient setting to test for linearity in an ordered disk packing. Specifically, to carry out such a test, we sampled points along the

lattice directions of a monodisperse hexagonal disk packing, which corresponds to the directions $x = \pm cz$ where the peaks of responses are located. In the CD model, the stresses at those points are only determined by the depth z , since $\sigma_{zz}(x \pm cz) = \frac{F}{4\sqrt{\pi D z}} e^{-\frac{c^2}{D} z}$. In Fig. 5(a), we plot the measured stress versus applied point force at different depths. We find that when the applied force is below about 0.5 N, there is a good linearity within the error bars. In our experiments, in order to increase the signal to noise ratio, we usually chose a working force close to the upper bound of this linear region.

A.3 Tests for linearity in disordered systems

The second model that is relevant here is the response of a semi-infinite elastic plate that is subject to an applied point force at the free surface, as sketched in Fig. 16. The stresses in this case are give by Eqs 8 and 9. In particular, Eq. 9 indicates a simple relationship for σ_{zz} that applies equally well to the other stress components in Cartesian coordinates: $\sigma_{zz}(0, z) = \frac{2F}{z\pi}$. Thus, we expect that $z\sigma_{zz}$ should depend linearly on F , for all depths. In Fig. 5(b), we plot the measured stress multiplied by the corresponding depth against the applied force. As expected, we see that lines for different depths collapse on the same line. However, this linearity only holds when the applied force is less than 0.5 N.

References

- [1] For a broad perspective see Focus Issue on Granular Materials, R. Behringer, H. Jaeger, S. Nagel, *Chaos* **9**, 509–696 (1999); *Physics of Dry Granular Media*, H. J. Herrmann, J.-P. Hovi, and S. Luding, eds. NATO ASI Series, Kluwer, 1997; *Powders and Grains 97*, R. P. Behringer and J. T. Jenkins, eds. Balkema, 1997; H. M. Jaeger, S. R. Nagel, and R. P. Behringer, *Rev. Mod. Phys.* **68**, 1259 (1996).
- [2] P.-G. de Gennes, *Rev. Mod. Phys.* **71**, 374 (1999).
- [3] G. Reydellet and E. Clément, *Phys. Rev. Lett.* **86**, 3308 (2001).
- [4] J. Geng, D. Howell, E. Longhi, R.P. Behringer, G. Reydellet, L. Vanel, E. Clément and S. Luding, *Phys. Rev. Lett.* **87**, 0335506 (2001).
- [5] M. Da Silva and J. Rajchenbach, *Nature (London)* **406**, 708 (2000).
- [6] J-P. Bouchaud, P. Claudin and D. Levine, M.Otto, *Euro. Phys. J.* **E4**, 451 (2001).
- [7] J.E.S. Socolar, D.G. Schaeffer, P. Claudin, *Euro. Phys. J.* **E7**, 353 (2002).

- [8] C. Goldenberg, I. Goldhirsch, Phys. Rev. Lett. **89**, 084302 (2002).
- [9] D. A. Head, A. V. Tkachenko, T. A. Witten, Euro. Phys. J. **E6**, 99 (2001).
- [10] A. V. Tkachenko and T. Q. Witten, Phys. Rev. E **60** 687 (1999).
- [11] A. V. Tkachenko and T. Q. Witten, Phys. Rev. E **62**, 2510 (2000).
- [12] N. W. Mueggenburg, H. M. Jaeger, and S. R. Nagel, Phys. Rev. E **66**, 031304 (2002).
- [13] C.F. Moukarzel, Granular Matter **3**, 41 (2001).
- [14] J. Duran, *Sands, Powders, and Grains: An Introduction to the Physics of Granular Materials* (Springer-Verlag, New York, 1999).
- [15] C. Eloy and E. Clément, J. Phys. I. France **7**, 1541 (1997).
- [16] L. Breton, P. Claudin, E. Clément, and J.-D. Zucker, Eruophys. Lett. **60**, 813 (2002).
- [17] C. Gay, R. da Silveira, preprint, cond-mat/0208155 (2002); R. da Silveira, G. Vidalenc, C. Gay, preprint, cond-mat/0208214 (2002).
- [18] P. Dantu, Géotechnique, **18**, 50 (1968); A. Drescher and G. De Josselin De Jong, J.Mech. Phys. Solids, **20**, 337 (1972); T. Travers et al. J. Phys. A. **19**, L1033 (1986).
- [19] D. M. Wood, *Soil Behaviour and Critical State Soil Mechanics* (Cambridge University, Cambridge, England, 1990); R. M. Nedderman, *Statics and Kinematics of Granular Materials*, Cambridge Univ. Press, Cambridge, 1992.
- [20] C.-h. Liu, S. R. Nagel, D. A. Schecter, S. N. Coppersmith, S. Majumdar, O. Narayan and T. A. Witten, Science **269**, 513 (1995), Phys. Rev. E **53**, 4673 (1996).
- [21] J.-P. Bouchaud, M. E. Cates, and P. Claudin, J. Phys. I, France **5**, 639 (1995); J. P. Wittmer, M. E. Cates, P. Claudin, J. Phys. R., France **7**, 39 (1997).
- [22] P. Claudin, J. P. Bouchaud, M. E. Cates, and J. P. Wittmer, Phys. Rev. E **57**, 4441 (1998).
- [23] M.E. Cates, J.P. Wittmer, J.-P. Bouchaud, and P. Claudin, Phys. Rev. Lett. **81**, 1841 (1998).
- [24] M. Otto, J.-P. Bouchaud, P. Claudin, and J. E. S. Socolar, Phys. Rev. E **67**, 031302 (2003).
- [25] J.D. Goddard, *Physics of Dry Granular Media*, pp.1-24, H. J. Herrmann, J.-P. Hovi, and S. Luding, eds. NATO ASI Series, Kluwer, (1998).
- [26] M. Latzel, S. Luding and H.J. Herrmann, Granular Matter **2**, 123 (2000).
- [27] L. Vanel, D. W. Howell, D. Clark, and R. P. Behringer, Phys. Rev. E Rapid Comm. **60**, R5040 (1999).

- [28] J. Geng, E. Longhi, R.P. Behringer and D. Howell, Phys. Rev. E **64**, 060301(R), 2001.
- [29] H.G. Matuttis, Gran. Mat. **1**, 83 (1998); H.G. Matuttis and A. Schinner, Gran. Mat. **1**, 195 (1999); H.G. Matuttis, S. Luding and H.J. Herrmann, Powder Technol. **109**, 278 (2000);
- [30] K. Liffman, M. Nguyen, G. Metcalfe and P. Cleary, Gran. Mat. **3**, 165 (2001).
- [31] R. B. Heywood, *Designing by Photoelasticity*. Chapman and Hall Ltd., London, (1952).
- [32] S. Luding, O. Strauß, in *Granular Gases*, T. Pöschel, and S. Luding eds., Springer-Verlag, Berlin, (2000).
- [33] J.M. Ziman, *Models of Disorder* (Cambridge University Press, Cambridge, (1979).
- [34] S. Wolfram, *The Mathematica Book*, Cambridge University Press, Cambridge, (1999); G. B. Wetherill, *Regression Analysis with Applications* (Chapman and Hall, New York, (1986).
- [35] L. Landau and E. Lifshitz, *Elasticity Theory*. Pergamon, New York, (1986).
- [36] D. Howell, C. Veje, and R. P. Behringer, Phys. Rev. Lett. **82**, 5241 (1999).
- [37] B. J. Miller, C. O'Hern, and R. P. Behringer, Phys. Rev. Lett. **77**, 3110 (1996).